AIAA JOURNAL
Vol. 35, No. 5, May 1997

Self-Contained Automated Methodology for Optimal Flow Control

Ronald D. Joslin,* Max D. Gunzburger,† and Roy A. Nicolaides‡
NASA Langley Research Center, Hampton, Virginia 23681-0001
and
Gordon Erlebacher§ and M. Yousuff Hussaini¶
Florida State University, Tallahassee, Florida 32306-4052

A self-contained, automated methodology for active flow control is described, which couples the time-dependent Navier–Stokes system with an adjoint Navier–Stokes system and optimality conditions from which optimal states, i.e., unsteady flowfields and controls (e.g., actuators), may be determined. The problem of boundary-layer instability suppression through wave cancellation is used as the initial validation case to test the methodology. Here, the objective of control is to match the stress vector along a portion of the boundary to a given vector; instability suppression is achieved by choosing the given vector to be that of a steady base flow. Control is effected through the injection or suction of fluid through a single orifice on the boundary. The results demonstrate that instability suppression can be achieved without any a priori knowledge of the disturbance, which is significant because other control techniques have required some knowledge of the flow unsteadiness such as frequencies, instability type, etc. The present methodology has been extended to three dimensions and may potentially be applied to separation control, relaminarization, and turbulence control applications using one to many sensors and actuators.

I. Introduction

In the last decade, increased attention has been devoted to the development of techniques capable of enhancing our ability to control the unsteady flow in a wide variety of configurations such as engine inlets and nozzles, combustors, automobiles, aircraft, and marine vehicles. Controlling the flow in these configurations can lead to greatly improved efficiency and performance, while decreasing the noise levels generally associated with the otherwise unattended unsteady flow. Depending on the desired result, one might wish to delay or accelerate transition, reduce drag or enhance mixing. There might be a need to postpone flow separation, increase lift, or manipulate a turbulence field. Gad-el-Hak[1] and Gad-el-Hak and Bushnell[2] provide an excellent introduction to and overview of various control methodologies.

Small improvements in system performance often lead to large payoffs. For example, Butter[3] estimates that a 5% improvement in landing maximum lift coefficient [C_l(max)] can translate to a 25% increase in payload. Cousteix[4] notes that 45% of the drag for a commercial transport transonic aircraft is due to skin friction on the wings, fuselage, fin, etc., and that a 10–15% reduction of the total drag can be expected by laminarizing the flow over the wings and the fin. This translates into a reduction in fuel requirements, improved performance, and/or increased payload. Muirhead[5] has shown with a wind-tunnel investigation that control of flow separation on a tractor-trailer truck can reduce the drag by 30–40% of the baseline truck configuration. This translates into a savings of millions of barrels of fuel per year.

Received Feb. 28, 1996; revision received Feb. 3, 1997; accepted for publication Feb. 12, 1997.

*Leader, Laminar Flow Control Project Team, Mail Stop 170. Member AIAA.
†Consultant, Institute for Computer Applications in Science and Engineering; currently Professor, Department of Mathematics, Iowa State University, Ames, IA 50011.
‡Consultant, Institute for Computer Applications in Science and Engineering; currently Professor, Department of Mathematics, Carnegie Mellon University, Pittsburgh, PA 15213.
§Assistant Professor of Mathematics. Member AIAA.
¶Eminent Scholar Chair in High Performance Computing.

Encouraged by the potential for huge rewards with what may be a modest input, research into ways of achieving these gains is ever important. In many applications, the flow starts from a smooth laminar state, which is inherently unstable, and develops instability waves. These instability waves grow exponentially, nonlinearly interacting, and lead ultimately to fully developed turbulence or flow seperation. Therefore, one goal of a good control system is to inhibit, if not eliminate, these instabilities, which lead to the deviation from laminar to turbulent flow state.

A. Wave-Cancellation Concept

The simplest form of control that might achieve this objective is the wave-cancellation approach, based on the premise that the instability mechanisms in low-speed transition are dominated by a single instability wave; therefore, canceling this wave will preclude the nonlinear interactions leading to laminar–turbulent transition. The wave-cancellation method further assumes that a wavelike disturbance can be canceled by introducing another wave equal in amplitude but opposite in phase and, thus, it is mostly applicable to systems governed by linear or quasilinear equations. The key is to determine the parameters of the downstream wave that counter (cancel) the evolution of the upstream generated wave. Because there are a number of experiments and numerical simulations that validate this approach, the wave-cancellation problem is an excellent test problem for the new flow-control methodology described in this paper.

Most of the experiments, aimed at verifying the wave-cancellation concept, were conducted on the flat plate, except those of Ladd and Hendricks,[6] Pupator and Saric,[7] and Ladd,[8] who considered axisymmetric bodies. Many of these experiments were conducted in water tunnels. Vibrating wires,[9] hot strips,[10,11] suction and blowing,[7,8] electromagnetic generators,[12] and adaptive heating[6] are some of the methods that were used to generate the controlling wave. All these input mechanisms give the necessary control of the phase and amplitude of the input wave. Among the more successful studies, Milling[9] and Thomas[12] achieved at least an 80% reduction in the input amplitude of the two-dimensional wave (with 0.6–1% amplitude). However, it was not possible to achieve relaminarization, probably because of the three dimensionality of the flow resulting from the interaction between background disturbances and the primary two-dimensional wave. As expected, the studies conducted on axisymmetric bodies produced relatively less wave cancellation because these flows are inherently three dimensional. Furthermore, good wave cancellation requires a linear system with constant

coefficients. This requirement is clearly violated for flow over a body with curvature. Liepmann and Nosenchuck[11] compared the effects of steady and nonsteady heating and found that steady heating demands a 2000% increase in energy over an unsteady wave-cancellation technique. Hence, unsteady control may be more efficient for flow control applications.

In addition to the aforementioned experiments, several theoretical (i.e., linear computations and theory) and computational studies (i.e., nonlinear simulations) have focused on understanding the physics of this wave-cancellation process. Maestrello and Ting[13] provided a linear asymptotic analysis to demonstrate the relationship between the input of localized disturbances and their effect on the Tollmien–Schlichting (TS) instability waves present in the wall-bounded shear flow. They showed that small amounts of local periodic heating could excite disturbances that actively control the TS waves that propagate in a boundary layer on a flat plate. Analogous to the experiments, several wave input mechanisms were considered. In one of the early Navier–Stokes simulations of active control, Biringen[14] used suction and blowing at the wall in a channel flow. He observed approximately a 50% reduction in the amplitudes of the two-dimensional instabilities and a decrease in the growth of the three-dimensional instabilities. The Reynolds stress originally generated by the waves was all but removed.

On the other hand, Metcalfe et al.[15] studied the effect of a moving wall on unstable waves traveling in a laminar flow on a flat plate. The simulations were based on the Navier–Stokes equations solved within a temporal framework. An energy analysis revealed that the wall motion causes the Reynolds-stress term to become negative, which implies a feed of energy from the perturbed flow back into the mean flow. In effect, this energy analysis showed how a perturbation to an unstable flow can be stabilizing. However, an instability wave eventually formed downstream of the control, with the same growth rate as the uncontrolled wave. This is a clear indication that the cancellation was not complete.

Although intuitively obvious, until the work of Bower et al.[16] and Pal et al.,[17] it was not known that perfect cancellation could be obtained within the context of linear theory (for which the mean flow is independent of the propagating direction). They used the two-dimensional Orr–Sommerfeld equation to study and control instability wave growth by superposition, and showed, within the limits of linear stability theory and the parallel flow assumption, that single and multifrequency waves can be canceled. The basic conclusions drawn by the early experimentalists were confirmed by the studies of Laurien and Kleiser[18] and Kral and Fasel.[19] They showed that it was possible to delay/accelerate transition by superposing disturbances out of/in phase with the primary TS wave. Similar results were also reported by Danabasoglu et al.[20] Finally, Joslin et al.[21] performed a numerical experiment that served to unequivocally demonstrate the link between linear superposition and instability suppression. To ensure that linear superposition of individual instabilities was, in fact, responsible for the results found in previous experiments and computations, they carried out three simulations with 1) only the disturbance, 2) only the control, and 3) both disturbance and control, which is the wave-cancellation case. By discretely summing the control only and forcing only numerical results, they found that this linear superposed solution is identical to the wave-cancellation results. These tests cleary verify the hypothesis that linear superposition is the reason for the previous experimental and computational results.

From these experiments, linear computations and nonlinear simulations, several common features emerge: 1) It is impossible to achieve perfect wave cancellation unless the system is linear, with constant coefficients; 2) the efficiency of wave cancellation decreases as the system becomes more nonlinear; 3) as the geometry of the configuration becomes more complex, cancellation becomes more difficult; and 4) the current approaches require foreknowledge of the instability wave characteristics, such as its frequency and amplitude before wave suppression can be realized.

B. Optimal Control Theory

The optimal control theory provides an approach that does not require a priori knowledge of the flow characteristics. The goal of optimal control theory is to minimize or maximize an objective function in a robust manner. When the flow is time dependent, and a strong function of initial conditions, it becomes difficult to establish the precise controls that will achieve the desired effect. Wave cancellation, as just discussed, only works well when the input wave has a dominant frequency and its properties are known. Then (either in a passive fashion or through a feedback mechanism), one seeks to cancel its effect while still in a linear regime. In practice, there are many waves, which can interact nonlinearly in ways not always known in advance. Rather than try to cancel the incoming waves, one seeks appropriate controls in other ways. One means of achieving this, without an extensive search over the space of possible controls, is to postulate a family of desired controls (e.g., an arbitrary time-dependent amplitude and a specified spatial distribution), and an objective function (i.e., stress over a region of the plate). Then, through a formal minimization process, one derives a set of differential equations and their adjoints, whose solution produces the optimal actuator profile (among the specified set). Although the solution to this set of equations cannot be accomplished in real time, the results can be applied using standard passive or active control mechanisms. The advantage of this approach is that entire collections of controls can be studied simultaneously, rather than one at a time.

Optimal control methodologies have been recently applied to a variety of problems involving drag reduction, flow, and temperature matching, etc., to provide more sophisticated flow control strategies in engineering applications. Computational fluid dynamics algorithms have reached a sufficiently high level of maturity, generality, and efficiency so that it is now feasible to implement sophisticated flow optimization methods, which lead to a large number of coupled partial differential equations. Optimal control theory is quite mathematical, and its formal nature is amenable to the derivation of mathematical theorems related to existence of solutions and well posedness of the problem. (Only partial results of this type are possible in three dimensions because, in this case, the Navier–Stokes equations themselves do not enjoy a full theoretical foundation; in two dimensions, a complete theory is available.) Two recent surveys of the mathematical theories of optimal flow control are Gunzburger[22] and Borggaard et al.[23] A mathematical study of a simplified problem related to the one considered in this paper can be found in Ref. 24.

Flows may also be controlled through controllers whose actuation is determined by feedback laws. For unsteady flows, including turbulent flows, feedback controls are considered, for example, in Refs. 25 and 26, as well as Ref. 27. Determining optimal feedback laws is a very difficult proposition, especially in the context of nonlinear problems, so that one usually has to be content with using suboptimal feedback laws. On the other hand, in our study, we consider optimal controllers as determined by optimal control methodologies instead of a feedback strategy.

Optimal control techniques will not provide the real-time control that one is ultimately interested in, but by systematically computing the best control within specified tolerances, with a given objective function, it will be possible to develop strategies (active or passive) to control a wide variety of disturbances. For example, to effectively control boundary-layer transition due to the interaction of a crossflow vortex and a TS wave using periodic heating and cooling, optimal control would 1) allow a determination of the best objective function to use for a given type of control (some are better than others) and 2) provide insight into the relationship between the time dependence of the control and the input waves. This insight could then be built into a neural network, or other type of self-learning system, to allow effective control over a wide range of input parameters.

C. Current Approach

The methodology is based on defining a control mechanism and an objective for control and then finding, in a systematic and automated manner, controls that best meet the objective. An objective or cost functional is defined that measures the distance between the measured stresses and their desired values along a limited section of the bounding wall and over a specified length of time. One may interpret the objective functional as a sensor, i.e., the objective functional senses how far the flow stresses along the wall are from the corresponding desired values. To control the flow, time-dependent injection and suction are imposed along a small orifice in the bounding wall. Although the spatial dependence of the suction

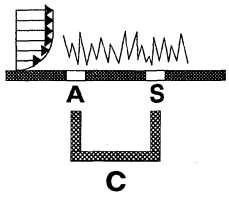

Fig. 1 Schematic of active flow control using optimal control theory: A, actuator; S, sensor; and C, control theory.

profile is specified (for simplicity), the optimal control methodology determines the time variation of this profile. However, unlike feedback control methodologies wherein the sensed data determine the control through a specified feedback law or controller, here the time dependence of the control is the natural result of the minimization of the objective functional. This scenario is shown in Fig. 1. We have a sensor that feeds information to a controller that in turn feeds information to the actuator. However, in the optimal control setting, the sensor is actually an objective functional and the controller is a coupled system of partial differential equations that determine the control that does the best job of minimizing the objective functional. The present active-control approach is demonstrated for the evolution and automated control of spatially growing two-dimensional disturbances in a flat-plate boundary layer. As the length of time over which the minimization process is increased, the results obtained by wave cancellation are recovered, thus validating the approach. The ultimate goal of this line of research is to introduce automated control to external flows over realistic configurations, such as wings and fuselages, and to devise novel flow control systems.

II. Optimization Problem

A. State Equations

Let Ω denote the flow domain, which is the semi-infinite channel or boundary layer $[x \geq 0, 0 \leq y \leq h]$, where h is the location of the upper wall for the channel or the truncated freestream distance for the boundary layer. Let Γ denote its boundary and let $(0, T)$ be the time interval of interest. The inflow part of the boundary $[x = 0, 0 \leq y \leq h]$ is denoted by Γ_i and the part of the boundary on which control is applied (i.e., along which the suction and blowing actuator is placed) by Γ_a, which is assumed to be a finite connected part of the lower boundary (or wall) $[x \geq 0, y = 0]$. Solid walls are denoted by Γ_w; for the channel flow, Γ_w is the lower boundary $[x \geq 0, y = 0]$ with Γ_a excluded and the upper boundary $[x \geq 0, y = h]$; for the boundary layer flow, Γ_w is only the lower boundary with Γ_a excluded. For the boundary-layer case, the upper boundary $[x \geq 0, y = h]$, which is not part of Γ_w, is denoted by Γ_e. Controls are only activated over the given time interval $t \in (T_0, T_1)$, where $0 \leq T_0 < T_1 \leq T$.

The flowfield is described by the velocity vector (u, v) and the scalar pressure p and is obtained by solving the following momentum and mass conservation equations:

$$\frac{\partial u}{\partial t} + u\frac{\partial u}{\partial x} + v\frac{\partial u}{\partial y} + \frac{\partial p}{\partial x} - \nu\frac{\partial}{\partial x}\left(2\frac{\partial u}{\partial x}\right) - \nu\frac{\partial}{\partial y}\left(\frac{\partial u}{\partial y} + \frac{\partial v}{\partial x}\right) = 0 \quad \text{in} \quad (0, T) \times \Omega \tag{1}$$

$$\frac{\partial v}{\partial t} + u\frac{\partial v}{\partial x} + v\frac{\partial v}{\partial y} + \frac{\partial p}{\partial y} - \nu\frac{\partial}{\partial x}\left(\frac{\partial u}{\partial y} + \frac{\partial v}{\partial x}\right) - \nu\frac{\partial}{\partial y}\left(2\frac{\partial v}{\partial y}\right) = 0 \quad \text{in} \quad (0, T) \times \Omega \tag{2}$$

$$\frac{\partial u}{\partial x} + \frac{\partial v}{\partial y} = 0 \quad \text{in} \quad (0, T) \times \Omega \tag{3}$$

subject to initial and boundary conditions

$$(u, v)|_{t=0} = (u_0, v_0) \quad \text{in} \quad \Omega \tag{4}$$

$$(u, v)|_{\Gamma_a} = \begin{cases} (g_1, g_2) & \text{in} \quad (T_0, T_1) \\ (0, 0) & \text{in} \quad (0, T_0) \quad \text{and} \quad (T_1, T) \end{cases} \tag{5}$$

$$(u, v)|_{\Gamma_i} = (u_i, v_i) \quad \text{and} \quad (u, v)|_{\Gamma_w} = (0, 0) \quad \text{in} \quad (0, T) \tag{6}$$

$$(u, v, p) \to \text{base flow}, \quad \frac{\partial u}{\partial x}, \frac{\partial v}{\partial x} \to 0 \quad \text{as} \quad x \to \infty \tag{7}$$

Here, the initial velocity vector $[u_0(x, y), v_0(x, y)]$ and the inflow velocity vector $[u_i(t, y), v_i(t, y)]$ are assumed given, and the base flow is assumed to be Poiseuille flow for the channel case and Blasius flow for the boundary-layer case. This system holds for both the channel and Blasius flow cases; in the latter case, the upper boundary is not part of Γ_w and the additional boundary condition

$$u|_{\Gamma_e} = U_\infty \quad \text{and} \quad p - 2\nu\frac{\partial v}{\partial y}\bigg|_{\Gamma_e} = P_\infty \quad \text{in} \quad (0, T) \tag{8}$$

is imposed, where U_∞ and P_∞ denote the freestream flow speed and pressure, respectively.

The control functions $g_1(t, x)$ and $g_2(t, x)$, which give the rate at which fluid is injected or sucked tangentially and perpendicularly, respectively, through Γ_a, are to be determined as part of the optimization process. To make sure that the control remains bounded at T_0, it is required that

$$g_1|_{t=T_0} = g_{10}(x) \quad \text{and} \quad g_2|_{t=T_0} = g_{20}(x) \quad \text{on} \quad \Gamma_a \tag{9}$$

where $g_{10}(x)$ and $g_{20}(x)$ are specified functions defined on Γ_a. Commonly, one chooses $g_{10}(x) = g_{20}(x) = 0$.

B. Objective Functional and the Optimization Problem

Assume that Γ_s is a finite, connected part of the lower boundary $[x \geq 0, y = 0]$, which is disjoint from Γ_a, and that (T_a, T_b) is a time interval such that $0 \leq T_a < T_b \leq T$. Then, consider the functional

$$\begin{aligned} \mathcal{J}(u, v, p, g_1, g_2) = {} & \frac{\alpha_1}{2}\int_{T_a}^{T_b}\int_{\Gamma_s} |\tau_1 - \tau_a|^2 \, d\Gamma \, dt \\ & + \frac{\alpha_2}{2}\int_{T_a}^{T_b}\int_{\Gamma_s} |\tau_2 - \tau_b|^2 \, d\Gamma \, dt \\ & + \frac{\beta_1}{2}\int_{T_0}^{T_1}\int_{\Gamma_a} \left(\left|\frac{\partial g_1}{\partial t}\right|^2 + |g_1|^2\right) d\Gamma \, dt \\ & + \frac{\beta_2}{2}\int_{T_0}^{T_1}\int_{\Gamma_a} \left(\left|\frac{\partial g_2}{\partial t}\right|^2 + |g_2|^2\right) d\Gamma \, dt \end{aligned} \tag{10}$$

where g_1 and g_2 denote the controls and $\tau_a(t, x)$ and $\tau_b(t, x)$ are given functions defined on $(T_a, T_b) \times \Gamma_s$. Note that since Γ_s is part of the lower boundary of the channel or boundary-layer wall, $\tau_1 = \nu\partial u/\partial y$ and $\tau_2 = -p + 2\nu\partial v/\partial y$ are the shear and normal stresses, respectively, exerted by the fluid on the bounding wall along Γ_s and, thus, τ_a and τ_b may be interpreted as given shear and normal stresses, respectively. Then, the boundary segment Γ_s can be thought of as a sensor, which measures the stresses on the wall. Thus, in Eq. (10), Γ_s is the part of the boundary Γ along which one wishes to match the shear and normal stresses to the given functions τ_a and τ_b, respectively, and (T_a, T_b) is the time interval over which this matching is to take place. (There are no difficulties, other than notational, introduced if one wishes to match each component of the stress vector over a different boundary segment and/or over a different time interval.)

The third and fourth terms in Eq. (10) are used to limit the size of the control. Indeed, no bounds are a priori placed on g_1 or g_2; their magnitudes are limited by adding a penalty to the stress matching functional defined by the first two terms in Eq. (10). The particular form that these penalty terms take, i.e., the third and fourth terms in Eq. (10), is motivated by the necessity to limit not only the size of the controls g_1 and g_2, but also to limit oscillations. The constants α_1, α_2, β_1, and β_2 can be used to adjust the relative importance of the terms appearing in the functional (10).

The (constrained) optimization problem is given as follows: Find u, v, p, g_1, and g_2 such that the functional $\mathcal{J}(u, v, p, g_1, g_2)$ given in Eq. (10) is minimized subject to the requirement that Eqs. (1–7) and (9) are satisfied and, for the boundary-layer flow case, Eq. (8) is also satisfied.

III. Optimality System

We first consider, in Secs. III.A–III.E, the case of a channel flow; the optimality system for the boundary layer flow is considered in Sec. III.F.

A. Lagrangian Functional

The method of Lagrange multipliers is formally used to enforce the constraints (1–3) and (5). To this end, the Lagrangian functional

$$\begin{aligned}
&\mathcal{L}(u, v, p, g_1, g_2, \hat{u}, \hat{v}, \hat{p}, s_1, s_2) \\
&= \frac{\alpha_1}{2}\int_{T_a}^{T_b}\int_{\Gamma_s} |\tau_1 - \tau_a|^2 \,d\Gamma\,dt + \frac{\alpha_2}{2}\int_{T_a}^{T_b}\int_{\Gamma_s} |\tau_2 - \tau_b|^2 \,d\Gamma\,dt \\
&+ \frac{\beta_1}{2}\int_{T_0}^{T_1}\int_{\Gamma_a}\left(\left|\frac{\partial g_1}{\partial t}\right|^2 + |g_1|^2\right) d\Gamma\,dt \\
&+ \frac{\beta_2}{2}\int_{T_0}^{T_1}\int_{\Gamma_a}\left(\left|\frac{\partial g_2}{\partial t}\right|^2 + |g_2|^2\right) d\Gamma\,dt - \int_0^T\int_\Omega \hat{u}\left[\frac{\partial u}{\partial t} + u\frac{\partial u}{\partial x}\right. \\
&\left. + v\frac{\partial u}{\partial y} + \frac{\partial p}{\partial x} - \nu\frac{\partial}{\partial x}\left(2\frac{\partial u}{\partial x}\right) - \nu\frac{\partial}{\partial y}\left(\frac{\partial u}{\partial y} + \frac{\partial v}{\partial x}\right)\right] d\Omega\,dt \\
&- \int_0^T\int_\Omega \hat{v}\left[\frac{\partial v}{\partial t} + u\frac{\partial v}{\partial x} + v\frac{\partial v}{\partial y} + \frac{\partial p}{\partial y} - \nu\frac{\partial}{\partial x}\left(\frac{\partial u}{\partial y} + \frac{\partial v}{\partial x}\right)\right. \\
&\left. - \nu\frac{\partial}{\partial y}\left(2\frac{\partial v}{\partial y}\right)\right] d\Omega\,dt - \int_0^T\int_\Omega \hat{p}\left(\frac{\partial u}{\partial x} + \frac{\partial v}{\partial y}\right) d\Omega\,dt \\
&- \int_{T_0}^{T_1}\int_{\Gamma_a} s_1(u - g_1)\,d\Gamma\,dt - \int_0^{T_0}\int_{\Gamma_a} s_1 u\,d\Gamma\,dt \\
&- \int_{T_1}^{T}\int_{\Gamma_a} s_1 u\,d\Gamma\,dt - \int_{T_0}^{T_1}\int_{\Gamma_a} s_2(v - g_2)\,d\Gamma\,dt \\
&- \int_0^{T_0}\int_{\Gamma_a} s_2 v\,d\Gamma\,dt - \int_{T_1}^{T}\int_{\Gamma_a} s_2 v\,d\Gamma\,dt \qquad (11)
\end{aligned}$$

is introduced. In Eq. (11), $\hat{u}$ and $\hat{v}$ are Lagrange multipliers that are used to enforce the x and y components of the momentum equations (1) and (2), respectively, $\hat{p}$ is a Lagrange multiplier that is used to enforce the continuity equation (3), and s_1 and s_2 are Lagrange multipliers that are used to enforce the x and y components of the boundary condition (5), respectively. Note that Lagrange multipliers have not been introduced to enforce the constraints (4), (6), (7), and (9), so that these conditions must be required of all candidate functions u, v, p, g_1, and g_2.

Through the introduction of Lagrange multipliers, the constrained optimization problem is converted into the following unconstrained problem: Find u, v, p, g_1, g_2, $\hat{u}$, $\hat{v}$, $\hat{p}$, s_1, and s_2 satisfying Eqs. (4), (6), (7), and (9) such that the Lagrangian functional $\mathcal{L}(u, v, p, g_1, g_2, \hat{u}, \hat{v}, \hat{p}, s_1, s_2)$ given by Eq. (11) is rendered stationary.

In this problem, each argument of the Lagrangian functional is considered to be an independent variable so that each may be varied independently.

The first-order necessary condition that stationary points must satisfy is that the first variation of the Lagrangian with respect to each of its arguments vanishes at those points. One easily sees that the vanishing of the first variations with respect to the Lagrange multipliers recovers the constraint equations (1–3) and (5). Specifically, $(\delta\mathcal{L}/\delta\hat{u}), (\delta\mathcal{L}/\delta\hat{v}) = 0 \Rightarrow x$- and y-momentum equations (1) and (2); $(\delta\mathcal{L}/\delta\hat{p}) = 0 \Rightarrow$ continuity equation (3); and $(\delta\mathcal{L}/\delta s_1), (\delta\mathcal{L}/\delta s_2) = 0 \Rightarrow x$ and y components of the boundary condition (5), where $\delta\mathcal{L}/\delta\hat{u}$ denotes the first variation of $\mathcal{L}$ with respect to $\hat{u}$, etc.

B. Adjoint Equations

Next, set the first variations of the Lagrangian with respect to the state variables u, v, and p equal to zero. These result in the adjoint or costate equations. Note that, because for the channel flow candidate solutions must satisfy Eqs. (4), (6), (7), and (9), one has that

$$\begin{aligned}
&\delta u|_{t=0} = \delta v|_{t=0} = 0 \quad \text{on} \quad \Omega, \qquad \delta g_2|_{t=T_0} = 0 \quad \text{on} \quad \Gamma_a \\
&\delta u|_{\Gamma_i} = \delta v|_{\Gamma_i} = 0; \qquad \delta u|_{\Gamma_w} = \delta v|_{\Gamma_w} = 0 \quad \text{for} \quad (0, T) \qquad (12) \\
&\delta p, \delta u, \delta v, \frac{\partial \delta u}{\partial x}, \frac{\partial \delta v}{\partial x} \to 0 \quad \text{as} \quad x \to \infty \quad \text{for} \quad (0, T)
\end{aligned}$$

First, consider $\delta\mathcal{L}/\delta p = 0$, which yields

$$\alpha_2\int_{T_a}^{T_b}\int_{\Gamma_s} \delta p(\tau_2 - \tau_b)\,d\Gamma + \int_0^T\int_\Omega \left(\hat{u}\frac{\partial \delta p}{\partial x} + \hat{v}\frac{\partial \delta p}{\partial y}\right) d\Omega\,dt = 0$$

for arbitrary variations δp in the pressure. Then applying Gauss' theorem yields that

$$\begin{aligned}
&\alpha_2\int_{T_a}^{T_b}\int_{\Gamma_s} \delta p(\tau_2 - \tau_b)\,d\Gamma - \int_0^T\int_\Omega \delta p\left(\frac{\partial \hat{u}}{\partial x} + \frac{\partial \hat{v}}{\partial y}\right) d\Omega\,dt \\
&+ \int_0^T\int_\Gamma \delta p(\hat{u}n_1 + \hat{v}n_2)\,d\Gamma\,dt = 0
\end{aligned}$$

where n_1 and n_2 denote the x and y components, respectively, of the outward normal to Ω along Γ. Choosing variations δp that vanish on the boundary Γ but that are arbitrary in the interior Ω of the flow domain yields that

$$\frac{\partial \hat{u}}{\partial x} + \frac{\partial \hat{v}}{\partial y} = 0 \quad \text{on} \quad (0, T) \times \Omega \qquad (13)$$

Now choosing variations δp that are arbitrary along the boundary Γ yields that

$$\hat{u}n_1 + \hat{v}n_2 = \begin{cases} 0 \quad \text{on} \quad (0, T) \times \Gamma\backslash\Gamma_s, (0, T_a) \times \Gamma_s, (T_b, T) \times \Gamma_s \\ -\alpha_2\left(-p + 2\nu\dfrac{\partial v}{\partial y} - \tau_b\right) \quad \text{on} \quad (T_a, T_b) \times \Gamma_s \end{cases} \qquad (14)$$

where $\Gamma\backslash\Gamma_s$ denotes the boundary Γ with Γ_s deleted. Note that in the preceding derivation of Eqs. (13) and (14), as in the derivations found subsequently, the boundary integrals at infinity do not make any contribution due to the last relation in Eq. (12).

Next, consider $\delta\mathcal{L}/\delta v = 0$, where Eq. (12) has been used to eliminate boundary integrals along Γ_i and Γ_w and as $x \to \infty$ and an integral over Ω at $t = 0$. First, variations δv that vanish at $t = 0$, $t = T$, and in a neighborhood of Γ are chosen, but which are otherwise arbitrary. Such a choice implies that all boundary integrals in Eq. (12) vanish, giving

$$\begin{aligned}
&-\frac{\partial \hat{v}}{\partial t} + \hat{u}\frac{\partial u}{\partial y} + \hat{v}\frac{\partial v}{\partial y} - u\frac{\partial \hat{v}}{\partial x} - v\frac{\partial \hat{v}}{\partial y} - \frac{\partial \hat{p}}{\partial y} - \nu\frac{\partial}{\partial x}\left(\frac{\partial \hat{u}}{\partial y} + \frac{\partial \hat{v}}{\partial x}\right) \\
&- \nu\frac{\partial}{\partial y}\left(2\frac{\partial \hat{v}}{\partial y}\right) = 0 \quad \text{in} \quad (0, T) \times \Omega \qquad (15)
\end{aligned}$$

where Eq. (3) is used to effect a simplification. Next, variations that vanish in a neighborhood of Γ, but which are otherwise arbitrary, are chosen to obtain

$$\hat{v}|_{t=T} = 0 \quad \text{in} \quad \Omega \qquad (16)$$

Now, along Γ, δv and $\partial\delta v/\partial n$ may be independently selected, provided that Eq. (12) is satisfied, where $\partial/\partial n$ denotes the derivative in the direction of the outward normal to Ω along Γ. If $\delta v = 0$ and $\partial\delta v/\partial n$ varies arbitrarily along Γ, then

$$\hat{v} = \begin{cases} 0 \quad \text{on} \quad (0, T) \times \Gamma\backslash\Gamma_s, (0, T_a) \times \Gamma_s, (T_b, T) \times \Gamma_s \\ \alpha_2\left(-p + 2\nu\dfrac{\partial v}{\partial y} - \tau_b\right) \quad \text{on} \quad (T_a, T_b) \times \Gamma_s \end{cases} \qquad (17)$$

To see this, note that along the inflow, Γ_i, $n_2 = 0$, and $\partial/\partial n = -\partial/\partial x$, whereas along the top and bottom boundaries $n_1 = 0$ and $\partial/\partial n = \pm\partial/\partial y$, respectively, and because $\delta v = 0$, $\partial\delta v/\partial x = 0$. Note that Eqs. (14) and (17) agree on the boundary segments where they simultaneously apply. Finally, δv is arbitrarily chosen along Γ_a to obtain

$$\begin{aligned}
s_2 = &-\hat{p}n_2 - \hat{v}(un_1 + vn_2) - \nu\left(\frac{\partial \hat{u}}{\partial y} + \frac{\partial \hat{v}}{\partial x}\right)n_1 \\
&- 2\nu\frac{\partial \hat{v}}{\partial y}n_2 \quad \text{on} \quad (0, T) \times \Gamma_a \qquad (18)
\end{aligned}$$

Next, consider $\delta\mathcal{L}/\delta u = 0$. Applying to the resulting equation, the same process that led to Eqs. (15–18) yields

$$-\frac{\partial \hat{u}}{\partial t} + \hat{u}\frac{\partial u}{\partial x} + \hat{v}\frac{\partial v}{\partial x} - u\frac{\partial \hat{u}}{\partial x} - v\frac{\partial \hat{u}}{\partial y} - \frac{\partial \hat{p}}{\partial x} - \nu\frac{\partial}{\partial x}\left(2\frac{\partial \hat{u}}{\partial x}\right) - \nu\frac{\partial}{\partial y}\left(\frac{\partial \hat{u}}{\partial y} + \frac{\partial \hat{v}}{\partial x}\right) = 0 \quad \text{in} \quad (0, T) \times \Omega \tag{19}$$

$$\hat{u}|_{t=T} = 0 \quad \text{in} \quad \Omega \tag{20}$$

$$\hat{u} = \begin{cases} 0 & \text{on} \quad (0, T) \times \Gamma \backslash \Gamma_s, (0, T_a) \times \Gamma_s, (T_b, T) \times \Gamma_s \\ \alpha_1\left(\nu\dfrac{\partial u}{\partial y} - \tau_a\right) & \text{on} \quad (T_a, T_b) \times \Gamma_s \end{cases} \tag{21}$$

and

$$s_1 = -\hat{p}n_1 - \hat{u}(un_1 + vn_2) - 2\nu\frac{\partial \hat{u}}{\partial x}n_1 - \nu\left(\frac{\partial \hat{u}}{\partial y} + \frac{\partial \hat{v}}{\partial x}\right)n_2 \quad \text{on} \quad (0, T) \times \Gamma_a \tag{22}$$

In deriving Eq. (21) we have used the assumption that Γ_s is part of the lower boundary of the channel so that along Γ_s we have that $n_2 = -1$. Again, there is no conflict between Eqs. (14) and (21) along boundary segments on which both apply.

C. Optimality Conditions

The only first-order necessary conditions left to consider are $\delta\mathcal{L}/\delta g_1 = 0$ and $\delta\mathcal{L}/\delta g_2 = 0$. (These conditions are usually called the optimality conditions.) Now, because all candidate functions g_1 and g_2 must statisfy Eq. (9), it follows that $\delta g_1 = 0$ and $\delta g_2 = 0$ at $t = T_0$. Then, take $\delta\mathcal{L}/\delta g_2 = 0$ and apply Gauss' theorem to remove all derivatives from the variation δg_2. Choosing variations δg_2 that vanish at $t = T_1$, but that are otherwise arbitrary, and using Eq. (18) yields

$$-\frac{\partial^2 g_2}{\partial t^2} + g_2 = -\frac{1}{\beta_2}\left(\hat{p} + 2\nu\frac{\partial \hat{v}}{\partial y}\right) \quad \text{on} \quad (T_0, T_1) \times \Gamma_a \tag{23}$$

where Eq. (17) and the assumption that Γ_a is part of the lower boundary so that, along Γ_a, $n_1 = 0$ and $n_2 = -1$ have been used. Now, choosing variations that are arbitrary at $t = T_1$ yields that $\partial g_2/\partial t = 0$ along Γ_a at $t = T_1$ so that, invoking Eq. (9), $g_2(t, x)$ satisfies

$$g_2|_{t=T_0} = g_{20}(x) \qquad \text{and} \qquad \left.\frac{\partial g_2}{\partial t}\right|_{t=T_1} = 0 \quad \text{on} \quad \Gamma_a \tag{24}$$

Note that, given $\hat{p}$ and $\hat{v}$, Eqs. (23) and (24) constitute, at each point $x \in \Gamma_a$, a two-point boundary value problem in time over the interval (T_0, T_1).

In a similar manner, setting $\delta\mathcal{L}/\delta g_1 = 0$ yields that

$$-\frac{\partial^2 g_1}{\partial t^2} + g_1 = -\frac{1}{\beta_1}\left(\nu\frac{\partial \hat{u}}{\partial y}\right) \quad \text{on} \quad (T_0, T_1) \times \Gamma_a \tag{25}$$

$$g_1|_{t=T_0} = g_{10}(x) \qquad \text{and} \qquad \left.\frac{\partial g_1}{\partial t}\right|_{t=T_1} = 0 \quad \text{on} \quad \Gamma_a \tag{26}$$

D. Finite Computational Domains

In the computations, the semi-infinite domain Ω (we are still only considering the channel flow case) is replaced by a finite domain Ω_C defined by the introduction of the outflow boundary Γ_o given by $[x = L, 0 \le y \le h]$. Thus, we have that Ω_C is the rectangle $[0 \le x \le L, 0 \le y \le h]$. The outflow does not require the imposition of boundary conditions along the outflow boundary Γ_o because a buffer zone[28] is attached to the end of the physical computational domain, where the governing equations are parabolized in this buffer region.

A similar treatment of the adjoint variables should have required consideration of an infinite domain $[-\infty < x < \infty, 0 < y < h]$. If this had been done, the boundary conditions (17) and (21) would not have been obtained along the inflow Γ_i. In fact, the inflow boundary Γ_i for the state equation is the outflow boundary for the adjoint equations, and, conversely, the outflow boundary Γ_o for the state equation is the inflow boundary for the adjoint equations. This is easily seen by comparing the leading inertial terms of the state equations with t increasing and the adjoint equations with t decreasing. Now, on both Γ_i and Γ_o we have that $u > 0$ and $v \approx 0$, which is why Γ_i is an inflow boundary and Γ_o is an outflow boundary for the state. On the other hand, the fact that t is decreasing in the adjoint equations implies that now Γ_i is an outflow boundary and Γ_o is an inflow boundary for those equations.

Thus, to be consistent with the treatment of the state equations, the adjoint outflow Γ_i should be treated in a manner similar to the preceding treatment of the state outflow Γ_o. This treatment of the adjoint outflow does not require the imposition of any boundary conditions for the adjoint variables along Γ_i. Finally, because Γ_o is an inflow boundary for the adjoint equations, one has that

$$\hat{u} = 0 \qquad \text{and} \qquad \hat{v} = 0 \quad \text{on} \quad (0, T) \times \Gamma_o \tag{27}$$

E. Optimality System for Channel Flow

We now have in hand the full optimality system for channel flow whose solutions determine the optimal states, controls, and adjoint states. These are state equations (1–7); costate equations (13–17), (19–21), and (27); and optimality equations (23–26).

Because Eqs. (18) and (22) merely serve to determine the uninteresting Lagrange multipliers s_2 and s_1, they can be ignored.

The state equations are driven by the given initial velocity (u_0, v_0), the given inflow velocity (u_i, v_i), and the controls (g_1, g_2). Indeed, the purpose of this study is to determine g_1 and g_2 that optimally counteracts instabilities created upstream of Γ_a. The adjoint equations are homogeneous except for the boundary condition along Γ_s, the part of the boundary along which we are trying to match the stresses. The data in that boundary condition are exactly the discrepancy between the desired stresses τ_a and τ_b and the stresses $\tau_1 = \nu\partial u/\partial y$ and $\tau_2 = -p + 2\nu\partial v/\partial y$ along Γ_s, weighted by the factors α_1 and α_2. The equations for the controls are driven by the negative of the adjoint stresses along Γ_a, the part of the boundary along which we apply the control, weighted by the factors $1/\beta_1$ and $1/\beta_2$. Of course, this division into equations for the state, the adjoint state, and the control is really obscured by the fact that the equations are all intimitately coupled.

F. Optimality System for Boundary-Layer Flow

Following a similar process to that used in Secs. III.A–III.E for the channel flow case, one may derive an optimality system for the boundary-layer flow case. The only difference is that in the latter case Γ_w denotes only the lower boundary with Γ_a excluded and that the additional boundary condition (8) along the upper boundary Γ_e must be accounted for.

With the new interpretation for Γ_w, one can still define the Lagrangian functional (11) and use the constraints (12) on allowable variations; however, due to Eq. (8), allowable variations are further constrained by

$$\delta u|_{\Gamma_e} = \left.\left(\delta p - 2\nu\frac{\partial \delta v}{\partial y}\right)\right|_{\Gamma_e} = 0 \quad \text{for} \quad (0, T)$$

which implies that, along Γ_e, one may not choose the variations in δp and $\partial\delta v/\partial y$ independently. Considering, simultaneously, variations in p, v, and $\partial v/\partial y$ along Γ_e, one can show that

$$\hat{u} = 0 \quad \text{on} \quad (0, T) \times \Gamma_e \tag{28}$$

Then, letting δv be arbitrary along Γ_e yields

$$\hat{p} + 2\nu\frac{\partial \hat{v}}{\partial y} + v\hat{v} = 0 \quad \text{on} \quad (0, T) \times \Gamma_e \tag{29}$$

The resulting system for boundary-layer flow now includes Eqs. (28) and (29), in addition to the channel flow system.

IV. Numerical Experiments

Here, the optimal control methodology developed in Sec. III is applied to a boundary-layer flow having a single instability wave that can be characterized by a discrete frequency within the spectrum. As described by Joslin et al.,[21,27] these discrete small-amplitude instabilities can be suppressed through wave cancellation (WC) using known information about the wave. Hence, the optimal control

is known for validation of the present direct numerical simulation (DNS)/optimal control theory numerical approach in which the instability is to be suppressed without any a priori knowledge of said instability.

We note that although we are testing our methodology and code for the special problem of two-dimensional TS wave suppression, that these were developed for the fully nonlinear Navier–Stokes system and, thus, are applicable to the case of nonlinear, three-dimensional waves. We would expect that more iterations, and perhaps a refined interation procedure, would be needed for convergence in a multimode case. Also, we have successfully suppressed a single large-amplitude TS wave; space limitations have prevented us from presenting these results here.

The formidable coupled system is solved in an iterative manner. First, the Navier–Stokes equations are solved for the state variables, i.e., the velocity field (u, v) and pressure p with control information (i.e., no control $g_1 = g_2 = 0$ for first iteration). Then costate equations are solved for the adjoint or costate variables $(\hat{u}, \hat{v})$ and $\hat{p}$. Then, using these adjoint variables, the controls g_1 and g_2 are then found by solving the optimality equations. The procedure is repeated until satisfactory convergence is achieved.

The nonlinear, unsteady Navier–Stokes equations and linear adjoint Navier–Stokes equations are solved by DNS of disturbances that evolve spatially within the boundary layer. The spatial DNS[29,30] approach involves spectral and high-order finite difference methods and a three-stage Runge–Kutta method[31] for time advancement. The influence-matrix technique is employed to solve the resulting pressure equation.[20,32] Disturbances are forced into the boundary layer by unsteady suction and blowing through a slot in the wall. The buffer-domain technique[28] is used for the outflow boundary treatment.

Only normal injection or suction control is allowed, so that we set $g_1 = 0$ in Eq. (5), $\beta_1 = 0$ in the functional (10), and ignore Eqs. (25) and (26). Also, we only match the normal stress along Γ_s so that we choose $\alpha_1 = 0$ in the functional (10) and in Eq. (21).

A. Computational Parameters

For the computations, the grid has 401 streamwise and 41 wall-normal points. The freestream boundary is located $75\delta_o^*$ from the wall, and the streamwise length is $224\delta_o^*$, which is equal to approximately 8 TS wavelengths. The nondimensional frequency for the forced disturbance is $F = \omega/Re \times 10^6 \doteq 86$; the forcing amplitude is $v_f = 0.1\%$. The Reynolds number based on the inflow displacement thickness (δ_o^*) is $Re = 900$. (The boundary segment along which disturbance forcing and control is affected as well as where stress matching occurs are located within the unstable region of the linear stability neutral curve.) A time-step size corresponding to 320 steps per period T_p is chosen for a three-stage Runge–Kutta method. Based on the disturbance frequency, a characteristic period can be defined as $T_p = 2\pi/\omega = 81.1781$; the resulting time-step size is then $\Delta t = 0.2537$.

To complete one period of the active-control simulation process, 0.75 min on the Cray C-90 are required using a single processor. Note, two periods of cost ($T_a \rightarrow T_b$ and $T_b \rightarrow T_a$) are required to complete one iteration of the DNS/adjoint system. Although, in general, any time interval may be specified for $T_a \rightarrow T_b$, this study uses integer increments of the period (T_p) for simplicity. Hence, $T_a \rightarrow T_b = 2T_p$ would cost $4T_p$ in computations, or roughly 3 min of C-90 time per iteration. Because only a single small-amplitude wave (linear) is forced, the grid is more than adequate; however, a grid refinement was performed and produced results equivalent to the results reported here.

For this study, the disturbance forcing slot Γ_f, the control or actuator orifice Γ_a, and the matching or sensor segment Γ_s have equal length $4.48\delta_o^*$. The forcing is centered downstream at $389.62\delta_o^*$ (the Reynolds number based on the displacement thickness at that location is $Re = 1018.99$), the actuator is centered at $403.62\delta_o^*$ ($Re = 1037.13$), and the sensor is centered at $417.62\delta_o^*$ ($Re = 1054.97$). These separation distances were arbitrarily chosen for this demonstration. In practice, the control and matching segments should have a minimal separation distance so that the pair can be packaged as a single unit, or bundle, for distributed application of many bundles.

B. Results

All simulations allow the flowfield to develop for one period, i.e., from $t = 0 \rightarrow T_a = T_p$ before control is initiated. In the first series of simulations, the interval during which control is applied is arbitrarily chosen to be $T_a \rightarrow T_b = 2T_p$. Based on $\alpha_1 = \beta_1 = 0$, $\alpha_2 = 1$, and $\beta_2 = 10$, the convergence history for the wall-normal velocity and measured normal shear τ_2 are shown in Fig. 2. The velocities are obtained at a fixed distance from the wall corresponding to $1.18\delta_o^*$ and at the fixed time T_b. Convergence is obtained with 4 iterations. The results demonstrate that a measure of wave cancellation can be obtained from the DNS/control theory system. The wall-normal amplitude of the modified wave at $Re = 1092.5$ is 40% of the uncontrolled wave; the control without optimizing the choice of α_1, α_2, β_1, and β_2 has led to a 60% decrease in the amplitude of the traveling wave. Clearly, Fig. 2 shows that a net reduction of the disturbance energy is obtained by energy input due to the control. This results in a delay of transition by way of a suppression of the instability evolution.

In the simulation, the control has been applied from $T_a \rightarrow T_b$ only; therefore, for $t > T_b$, Eq. (5) indicates that the actuation is discontinued. Figure 3 compares velocity profiles at $Re = 1073.2$ for the converged results (C1) of Fig. 2 with results for one period after control $t = T_b + T_p$. The measured disturbance tends toward the uncontrolled solution when the actuation is discontinued (as expected); because the control was applied for $T_a = T_p \rightarrow T_b = 2T_p$,

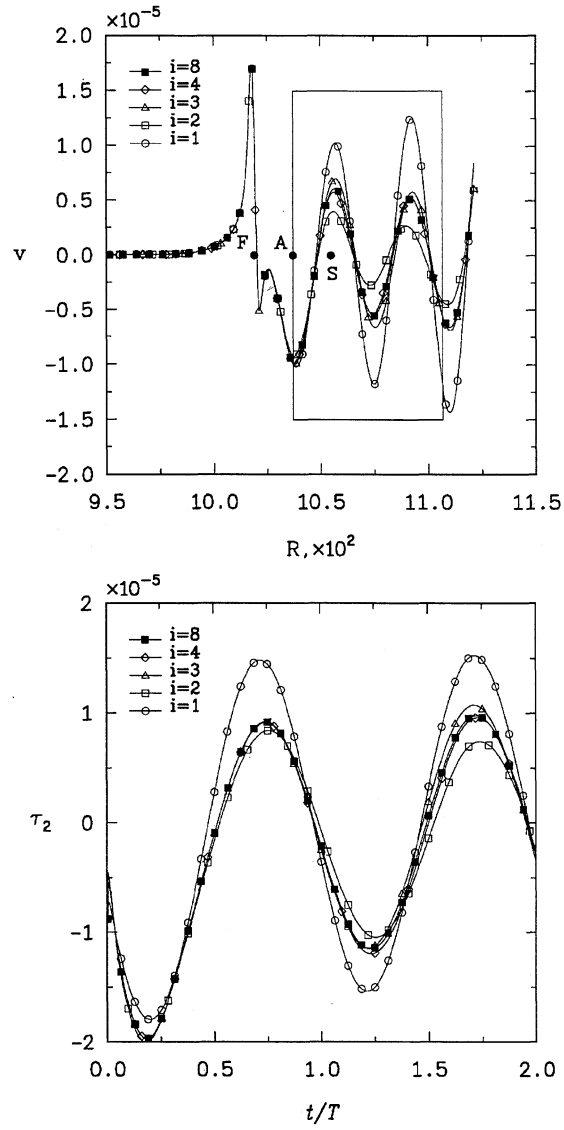

Fig. 2 Convergence of disturbance wall-normal velocity with downstream distance and sensor-measured shear stress with discrete time for control in flat-plate boundary-layer flow; velocity signal at $y = 1.18\delta_o^*$ from wall; $T_1 - T_0 = 2T_p$.

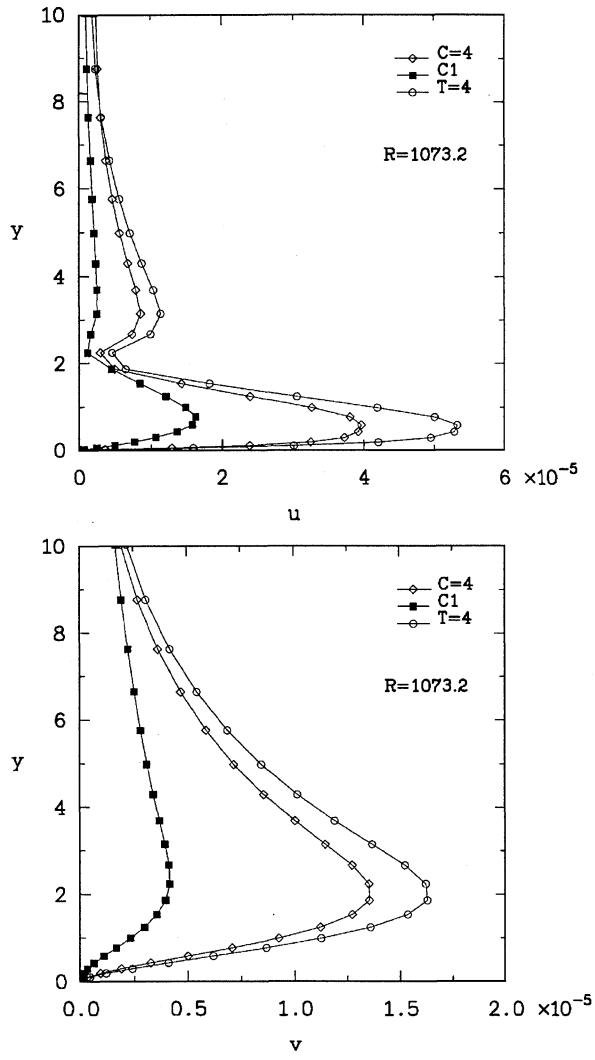

Fig. 3 Disturbance velocity profiles for no control (T = 4), control (C1), and after control is used and turned off (C = 4) in flat-plate boundary-layer flow.

two periods are required after T_b before the computed solution in the window exactly matches the uncontrolled solution. Clearly, the control only removes energy from the system (decreases the wave instability amplitude); the resulting profiles retain the expected instability profile shape.

The effect of varying the window size (T_a, T_b) is demonstrated. The previous converged results (C1) are shown with converged results (C2) for the extended window ($T_a = T_p \rightarrow T_b = 3T_p$). The results are identical for the first two periods of time and indicate that extending the amount of time for control serves to extend control only. This result also indicates that one can solve for the optimal control over a given time interval (T_a, T_b) by breaking up that interval and solving for the optimal control over a series of smaller subintervals. This approach usually leads to substantial savings in CPU and memory costs. An additional insight about the present DNS/control theory is gleamed by the increased temporal frame. The resulting optimal control g_2 approaches the desired WC time-periodic solution as the temporal length (T_a, T_b) is increased. This is convincing evidence that the present self-contained methodology is valid.

The instability wave resulting from WC is shown with the control (C2) in Figs. 4 and 5. For the present comparison, the amplitude of the actuation for WC was adjusted until nearly exact WC was achieved. Although the DNS/control theory did not achieve the same level of energy removal, the similar effect of WC was achieved without any a priori knowledge of the instability. Also, note that Fig. 5 shows that the optimal control of the control theory has nearly the exact phase characteristics as WC and only lacks the necessary amplitude for additional wave cancellation. These encouraging results suggest that by the appropriate selection of α_1, α_2, β_1, and β_2, the

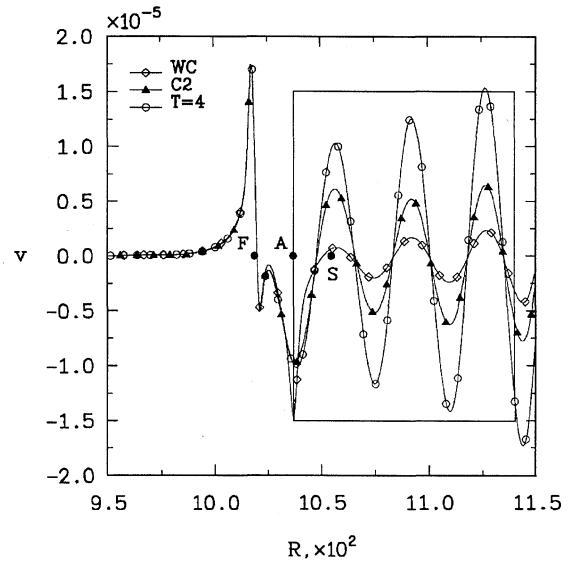

Fig. 4 Disturbance velocity with downstream distance for no control (T = 4), control (C2), and WC in flat-plate boundary-layer flow; velocity signal at $y = 1.18\delta_o^*$ from wall; $T_1 - T_0 = 3T_p$.

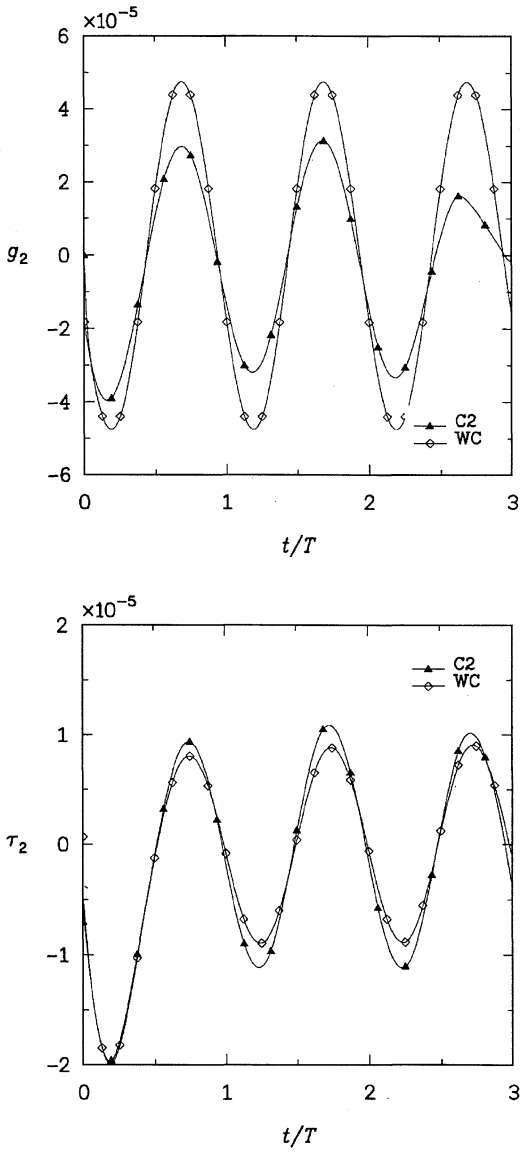

Fig. 5 Actuator response and sensor-measured shear stress for control (C2) and WC with discrete time.

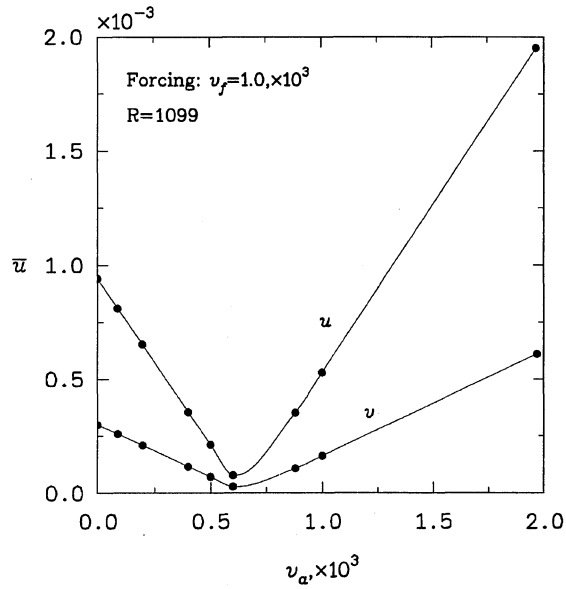

Fig. 6 Disturbance velocity resulting from variations in actuator amplitude from simulations in Ref. 21.

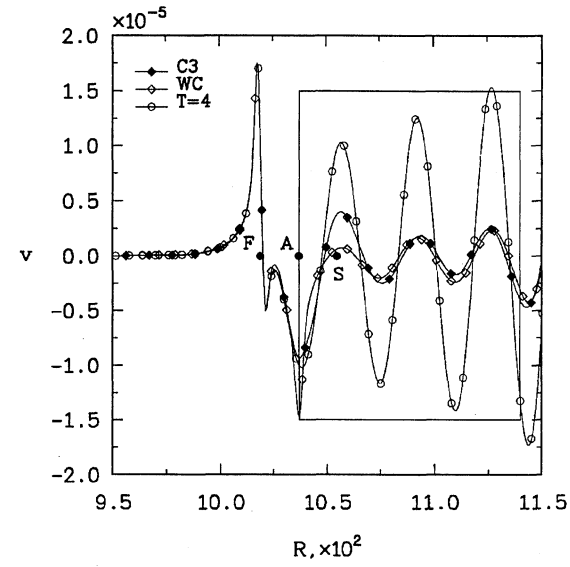

Fig. 7 Disturbance velocity with downstream distance for no control (T = 4), control (C3), and WC in flat-plate boundary-layer flow; velocity signal at $y = 1.18\delta_o^*$ from wall; $T_1 - T_0 = 3T_p$.

optimal control can be made nearly as effective a method of instability suppression as exact WC.

From the WC study of Joslin et al.,[21] the relationship between amplitude of the actuator (v_a) with resulting instabilty can be shown in Fig. 6. A similar result was shown in the channel flow WC study in Biringen.[14] The trend indicates that beginning with a small-actuation amplitude, as the actuation level is increased, the amount of WC (energy extraction from the disturbance) increases. At some optimal actuation, nearly exact WC is achieved for the instability wave. As the actuation amplitude further increases the resulting instability amplitude increases; this was clearly explained in Ref. 21 to occur because in the wave superposition process, the actuator wave becomes dominant over the forced wave. At this point, the resulting instability undergoes a phase shift corresponding to the phase of the wave generated by the actuator. The relationship depicted in Fig. 6 is encouraging for the DNS/optimal control theory approach and suggests that a gradient descent type algorithm might further enhance the wave suppression capability of the present approach. Namely, an approach for the optimal selection of α_1, α_2, β_1, and β_2 might lead to a more useful theoretical/computational tool for flow control.

To simply demonstrate this concept, Lagrange interpolation (or perhaps extrapolation) is introduced for β_1 and β_2 based on imposed values for α_1 and α_2:

$$\beta_{1,2}^{n+1} = \frac{\beta_{1,2}^{n}\left(\tau_{1,2}^{*} - \tau_{1,2}^{n-1}\right) - \beta_{1,2}^{n-1}\left(\tau_{1,2}^{*} - \tau_{1,2}^{n}\right)}{\left(\tau_{1,2}^{n} - \tau_{1,2}^{n-1}\right)} \tag{30}$$

where $\tau_{1,2}^{*}$ are some desired values of the stress components and $\tau_{1,2}^{n}$ are the stress components based on the choice $\beta_{1,2}^{n}$. Although τ_1^* and τ_2^* may be equivalent to the target values τ_a and τ_b in the functional (10), this may lead to significant over/undershoots for the interation process. Instead, τ_1^* and τ_2^* is the incremental decrease, or target value, for interpolation to more desirable β_1 and β_2 values. To illustrate this process, the $\beta_2 = 10$ (C2) and $\beta_2 = 11$ control results are obtained with the iteration procedure. The measures of normal stress are somewhat arbitrarily obtained at some time as measured by the sensor or matching segment Γ_s; the values of the normal stress are given in the Table 1. These values are used for a desired normal stress τ_2^*, which in this case is 65% of the $\beta_2 = 11$ results.

Using the results for $\beta_2 = 10$ and $\beta_2 = 11$ in Eq. (30) yields the value $\beta_2 = 16.5$, which is used in a simulation to obtain a greater degree of instability suppression. The WC results and the enhanced optimal control (C3) solution are shown in Figs. 7 and 8. This interpolation approach based on relationship of Fig. 6 indicates that optimizing β_2 has led to results very close to WC. The solutions differ somewhat near $t = T_a$ and $t = T_b$ because of the conditions (24) and (26) that serve to control the levels of g_1 and g_2. For all prac-

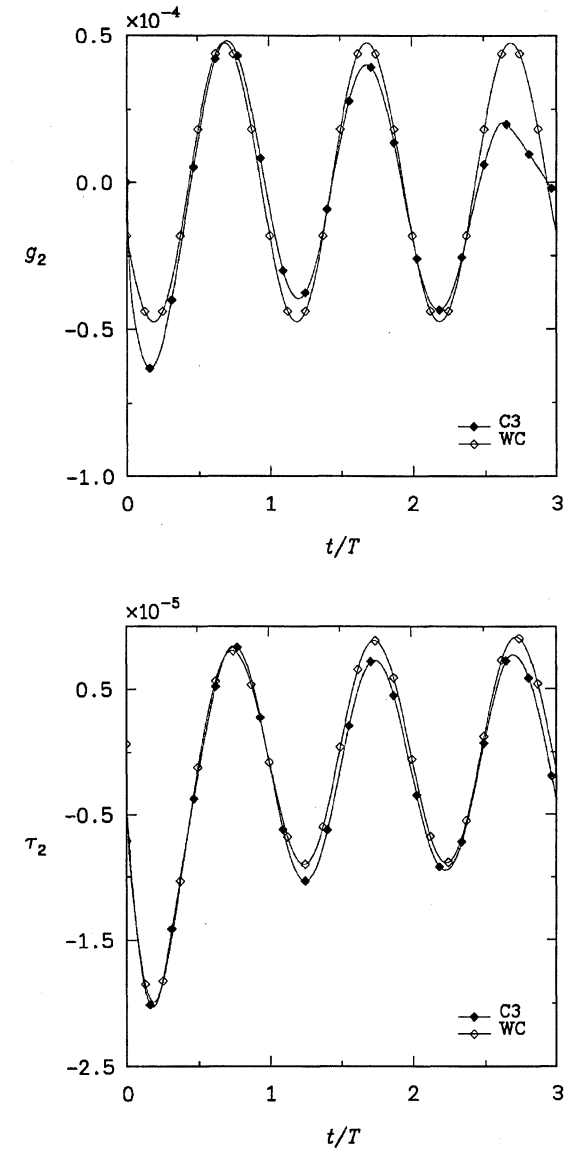

Fig. 8 Actuator response and sensor-measured shear stress for control (C3) and WC with discrete time.

Table 1 Normal stress for two values of β_2

β_2	Normal stress
10	9.369×10^{-6}
11	8.814×10^{-6}

tical purposes, the solutions obtained with the present DNS/control theory methodology yield the desired flow control features without prior knowledge of the forced instability.

The adjoint system requires that the velocity field (u, v) obtained from the Navier–Stokes equations be known for all time. For the iteration sequence and a modestly coarse grid, 82 Mbytes of disk (or runtime) space are required to store the velocities at all time steps and for all grid points. For $T_a \rightarrow T_b = 3T_p$, 246 Mbytes are necessary for the computation. Clearly, for three-dimensional problems the control scheme becomes prohibitively expensive. Therefore, a secondary goal of this study is to determine whether this limitation can be eliminated.

Because the characteristics of the actuator (g_1 and g_2) and resulting solutions are comparable to WC, some focus should be placed on eliminating the enormous memory requirements just discussed. This limitation can easily be removed if the flow control problem involves small-amplitude unsteadiness (or instabilities). The time-dependent coefficients of the adjoint systems (15) and (19) reduce to the steady-state solution, and no additional memory is required over the Navier–Stokes system in terms of coefficients. This has been verified by a comparison of a simulation with steady coefficients compared with the C2 control case. The results for both cases are identical (as expected). Additionally, if the instabilities have small amplitudes, then a linear Navier–Stokes solver can be used instead of the full nonlinear solver, which was used in the present study. This linear system would be very useful for the design of flow control systems. However, if the instabilities in the flow have sufficient amplitude to interact nonlinearly, then some measure of unsteady coefficient behavior is likely required. Depending on the amplitudes, the coefficients saved at every time step may be replaced with storing coefficients every 10 or more time steps thereby reducing the memory requirements by an order of magnitude. This hypothesis will require validation in a future study.

Conclusions

The coupled Navier–Stokes equations, adjoint Navier–Stokes equations, and optimality condition equations were solved and validated for the flow control problem of instability wave suppression in a flat plate boundary layer. By solving the described system, optimal controls were determined that met the objective of minimizing the perturbation normal stress along a portion of the bounding wall. As a result, the optimal control was found to be an effective means for suppressing two-dimensional, unstable Tollmien–Schlichting traveling waves. The results indicate that the DNS/control theory solution is comparable to the WC result but, unlike the latter, requires no a priori knowledge of the instability characteristics.

Acknowledgments

This research was supported by NASA under Contract NAS1-19480 while the authors (except the first author) were in residence at the Institute for Computer Applications in Science and Engineering, NASA Langley Research Center, Hampton, Virginia. Max Gunzburger was also supported by the U.S. Air Force Office of Scientific Research under Grant AFOSR-93-1-0280.

References

[1]Gad-el-Hak, M., "Flow Control," *Applied Mechanics Review*, Vol. 42, No. 10, 1989, pp. 261–293.

[2]Gad-el-Hak, M., and Bushnell, D. M., "Separation Control: Review," *Journal of Fluids Engineering*, Vol. 113, No. 1, 1991, pp. 5–30.

[3]Butter, D. J., "Recent Progress on Development and Understanding of High-Lift Systems," AGARD-CP-365, Aug. 1984.

[4]Cousteix, J., "Basic Concepts on Boundary Layers," AGARD-R-786, March 1992.

[5]Muirhead, V. U., "An Investigation of Drag Reduction for Tractor-Trailer Vehicles," NASA CR 144877, Oct. 1978.

[6]Ladd, D. M., and Hendricks, E. W., "Active Control of 2-D Instability Waves on an Axisymmetric Body," *Experiments in Fluids*, Vol. 6, No. 1, 1988, pp. 69, 70.

[7]Pupator, P., and Saric, W., "Control of Random Disturbances in a Boundary Layer," AIAA Paper 89-1007, March 1989.

[8]Ladd, D. M., "Control of Natural Laminar Instability Waves on an Axisymmetric Body," *AIAA Journal*, Vol. 28, No. 2, 1990, pp. 367–369.

[9]Milling, R. W., "Tollmien-Schlichting Wave Cancellation," *Physics of Fluids*, Vol. 24, No. 5, 1981, pp. 979–981.

[10]Liepmann, H. W., Brown, G. L., and Nosenchuck, D. M., "Control of Laminar-Instability Waves Using a New Technique," *Journal of Fluid Mechanics*, Vol. 118, May 1982, pp. 187–200.

[11]Liepmann, H. W., and Nosenchuck, D. M., "Active Control of Laminar-Turbulent Transition," *Journal of Fluid Mechanics*, Vol. 118, May 1982, pp. 201–204.

[12]Thomas, A. S. W., "The Control of Boundary-Layer Transition Using a Wave-Superposition Principle," *Journal of Fluid Mechanics*, Vol. 137, Dec. 1983, pp. 233–250.

[13]Maestrello, L., and Ting, L., "Analysis of Active Control by Surface Heating," AIAA Paper 84-0173, Jan. 1984.

[14]Biringen, S., "Active Control of Transition by Periodic Suction-Blowing," *Physics of Fluids*, Vol. 27, No. 6, 1984, pp. 1345–1347.

[15]Metcalfe, R. W., Rutland, C., Duncan, J. H., and Riley, J. J., "Numerical Simulations of Active Stabilization of Laminar Boundary Layers," AIAA Paper 85-0567, March 1985.

[16]Bower, W. W., Kegelman, J. T., Pal, A., and Meyer, G. H., "A Numerical Study of Two-Dimensional Instability-Wave Control Based on the Orr-Sommerfeld Equation," *Physics of Fluids*, Vol. 30, No. 4, 1987, pp. 998–1004.

[17]Pal, A., Bower, W. W., and Meyer, G. H., "Numerical Simulations of Multifrequency Instability-Wave Growth and Suppression in the Blasius Boundary Layer," *Physics of Fluids A*, Vol. 3, No. 2, 1991, pp. 328–340.

[18]Laurien, E., and Kleiser, L., "Numerical Simulation of Boundary-Layer Transition and Transition Control," *Journal of Fluid Mechanics*, Vol. 199, Feb. 1989, pp. 403–440.

[19]Kral, L. D., and Fasel, H. F., "Numerical Investigation of the Control of the Secondary Instability Process in Boundary Layers," AIAA Paper 89-0984, March 1989.

[20]Danabasoglu, G., Biringen, S., and Streett, C. L., "Spatial Simulation of Instability Control by Periodic Suction and Blowing," *Physics of Fluids A*, Vol. 3, No. 9, 1991, pp. 2138–2147.

[21]Joslin, R. D., Erlebacher, G., and Hussaini, M. Y., "Active Control of Instabilities in Laminar Boundary-Layer Flow. An Overview," NASA CR 195016, ICASE Rept. 94-97, Dec. 1994.

[22]Gunzburger, M., *Flow Control*, Springer, Berlin, 1995, pp. 1–381.

[23]Borggaard, J., Burkardt, J., Gunzburger, M., and Peterson, J., *Optimal Design and Control*, Birhäuser, Boston, 1995, pp. 1–286.

[24]Fursikov, A. V., Gunzburger, M., and Hou, L., "Boundary Value Problems and Optimal Boundary Control of the Navier–Stokes System: The Two-Dimensional Case," *Journal of Control Optimization* (to be published).

[25]Choi, H., Temam, R., Moin, P., and Kim, J., "Feedback Control of Unsteady Flow and Its Application to the Stochastic Burgers Equation," *Journal of Fluid Mechanics*, Vol. 253, Aug. 1993, pp. 509–543.

[26]Bewley, T., Moin, P., and Temam, R., "A Method for Optimizing Feedback Control Rules for Wall Bounded Turbulent Flows Based on Control Theory," *Forum on Control of Transition and Turbulent Flows*, ASME Fluids Engineering Conf., San Diego, FED-Vol. 237, 1996, pp. 279–286.

[27]Joslin, R. D., Nicolaides, R. A., Erlebacher, G., Hussaini, M. Y., and Gunzburger, M., "Active Control of Boundary-Layer Instabilities: Use of Sensors and Spectral Controller," *AIAA Journal*, Vol. 33, No. 8, 1995, pp. 1521–1523.

[28]Streett, C. L., and Macaraeg, M. G., "Spectral Multi-Domain for Large-Scale Fluid Dynamics Simulations," *Applied Numerical Mathematics*, Vol. 6, 1989, pp. 123–140.

[29]Joslin, R. D., Streett, C. L., and Chang, C.-L., "Validation of Three-Dimensional Incompressible Spatial Direct Numerical Simulation Code—A Comparison with Linear Stability and Parabolic Stability Equations Theories for Boundary-Layer Transition on a Flat Plate," NASA TP-3205, July 1992.

[30]Joslin, R. D., Streett, C. L., and Chang, C.-L., "Spatial Direct Numerical Simulation of Boundary-Layer Transition Mechanisms: Validation of PSE Theory," *Theoretical and Computational Fluid Dynamics*, Vol. 4, No. 6, 1993, pp. 271–288.

[31]Williamson, J. H., "Low-Storage Runge–Kutta Schemes," *Journal of Computational Physics*, Vol. 35, No. 1, 1980, pp. 48–56.

[32]Streett, C. L., and Hussaini, M. Y., "A Numerical Simulation of the Appearance of Chaos in Finite-Length Taylor-Couette Flow," *Applied Numerical Mathematics*, Vol. 7, No. 1, 1991, pp. 41–71.

J. Kallinderis
Associate Editor